ETH
Eidgenössische Technische Hochschule Zürich
Swiss Federal Institute of Technology Zurich

Autonomous Systems Lab
Prof. Roland Siegwart

Bachelor Thesis

Traction Control Concepts for a Walking Excavator

Autumn Term 2015

Supervised by:
Prof. Dr. Marco Hutter

Author:
Simon Zimmermann

Declaration of Originality

I hereby declare that the written work I have submitted entitled

Traction Control Concepts for a Walking Excavator

is original work which I alone have authored and which is written in my own words.[1]

Author(s)

Simon	Zimmermann

Student supervisor(s)

Marco	Hutter

Supervising lecturer

Roland	Siegwart

With the signature I declare that I have been informed regarding normal academic citation rules and that I have read and understood the information on 'Citation etiquette' (`https://www.ethz.ch/content/dam/ethz/main/education/rechtliches-abschluesse/leistungskontrollen/plagiarism-citationetiquette.pdf`). The citation conventions usual to the discipline in question here have been respected.

The above written work may be tested electronically for plagiarism.

Place and date	Signature

[1] Co-authored work: The signatures of all authors are required. Each signature attests to the originality of the entire piece of written work in its final form.

Contents

Abstract

This bachelor thesis presents the development and comparison of different traction control concepts for a 12 ton walking excavator with the purpose of increasing its climbing abilities, control and performance while driving through challenging terrain. In order to reach this goal, different existing traction control strategies have been studied and compared. Out of that, the *Slip Minimization* strategy has been found to be the best possible strategy in order to improve the traction behaviour of the excavator. As a first step to realise this approach, a quasi-static excavator model has been developed and its functionality has been simulated with a simple MATLAB script. This simulation shows reasonable results and validates the performance of the derived model.

Symbols

Symbols

V_w	wheel speed
V	vehicle speed
λ	slip ratio
$\dot{\lambda}$	slip ratio change
ϵ	denominator parameter
μ	friction coefficient
J	inertia
ω	wheel rotation
$\dot{\omega}$	wheel acceleration
M	motor torque
r	wheel radius
F_d	driving / friction force
m	vehicle mass
N	normal force
F_{dr}	driving resistance
κ	controller gain
τ	controller time constant
s	frequency (in frequency domain)
F_m	acceleration command (driver pedal)
a_c	curve gradient
F_{air}	air resistance force
F_{res}	rolling resistance force
F_z	ground contract force
s_{slide}	sliding surface
η	strictly positive constant
C_i	constant coefficients
P	plant
α	relaxation factor
T	traction force
$\boldsymbol{V_i}$	vector wheel-ground contact point to vehicle's center of mass
P_i	wheel-ground contact point
S	vehicle's center of mass
F_x, F_y	forces acting on vehicle's center of mass
M_z	torque acting on vehicle's chassis

$\boldsymbol{F}$	vector of vehicle's center of mass forces / torque
$\boldsymbol{f}$	vector of wheel-ground contact forces
γ_i	wheel-ground contact angle for wheel i
G	geometric matrix

Indices

w	wheel
max	maximum
0	operation point
d	desired
x	x axis
y	y axis
z	z axis

Acronyms and Abbreviations

ETH	Eidgenössische Technische Hochschule
ASL	Autonomous Systems Lab
KTI	Kommission für Technologie und Innovation
GPS	Global Positioning System
RLS	Recursive Least Squares
SRE	Slip Ratio Estimation
SRC	Slip Ratio Control
PI	Proportional-Integral
SMC	Sliding-mode Control
FCE	Friction Coefficient Estimation
MFC	Model Following Control
UOT	University of Tokyo
LPF	Low-pass Filter
HPF	High-pass Filter
MTTE	Maximum Transmissible Torque Estimation

List of Figures

List of Tables

Chapter 1

Introduction

Walking excavators belong to one of the most versatile excavator types. This versatility comes with the price of making these mobile construction site machines quite complex due to many joints and degrees of freedom. They are developed for different working tasks that require advanced mobility. Examples are excavating works in hardly accessible areas like mountains and rivers. The object of research of this work is the walking excavator M545 (depicted in figure 1.1)developed by the Swiss excavator supplier Menzi Muck AG [6]. Detailed information about the structure and the driving concept of this excavator can be found in [7].

Figure 1.1: Menzi Muck's walking excavator M545; Source: [1]

The presented work is part of a KTI project of the Autonomous Systems Lab (ASL) of ETH Zurich [8] and Menzi Muck AG. The project goal is to automate walking excavators using control and optimization tools that were developed and tested with legged robots. The shared vision is to enhance the intelligence of these machines such that they can drive or walk on rough terrain autonomously or with little human input.

In the ongoing work of this project, force control tools have been developed that allow to actively adapt the chassis as a function of the terrain. This has the purpose of optimizing the ground reaction force distribution for better stability, less terrain damage and reduction of operation complexity. Detailed information can be found in [9].
As a further step of the project, it is planned to increase the excavator's maximum reachable velocity in order to extend its applicability. As a first step to reach this goal, different fast driving concepts have been developed and compared. The results can be found in [7].
The walking excavator is conceived to do excavating work in hardly reachable places. In order to that, it often has to drive over rough and challenging terrain. That is why a good traction behaviour of the wheels is important. In the current excavator version, there is the problem that it often starts to skid when it has to climb hills with high inclinations and loose soil. Out of that, the goal of this *bachelor thesis* is to do a first step towards improving the excavator's traction behaviour in order to improve its climbing abilities, control and performance. To reach this goal, different traction control concepts have been studied and compared. It is omitted to itemize these concepts in this introduction, as it will be explained in the progress of this thesis.
The excavator gives a good basis to perform traction control, as the M545 type has an all-wheel drive system, based on wheel hub drives (more in [7]). This leads to the advantage that each wheel can be controlled separately.

Chapter 2

Traction Control Concepts

In this chapter, an overview of different traction control concepts will be given that have been developed until now. First of all, an introduction regarding wheel slip and longitudinal motion dynamics of a vehicle will be given in section 2.1. Afterwards, the ideas of different traction control strategies and methods will be presented and compared in the sections 2.2 and 2.3.
It is not the aim of this documentation to fully describe each single strategy completely. The intent is to give an overview and present the basic ideas of the today's existing traction control concepts.

2.1 Introduction

2.1.1 Slip Control

There are different factors that can be adjusted in order to improve the traction behaviour of a vehicle. According to [10], the main factors that affect the traction efficiency are the tire pressure, the vertical load of the vehicle's wheels as well as properties of tires and ground and their interaction. The main possibilities of improving the traction behaviour therefore include slip control, dynamic vertical load adjustment and automatic tyre pressure control. As the two last named methods remain technically difficult, this thesis focuses on slip control.
Before we can start with the control of this parameter, we first have to understand what it is. In general, wheel slip is defined as the difference between vehicle and wheel velocities. To express this relation, the longitudinal slip ratio can be defined as (according to [4]):

$$\lambda = \frac{V_w - V}{max(V_w, V, \epsilon)} \tag{2.1}$$

where $V_w = \omega \cdot r$ is the wheel rotational speed (with wheel radius r and the angular wheel speed ω) and V is the longitudinal vehicle speed. $\epsilon << 1$ is included to ensure that the denominator is never zero.
According to [11], slip occurs whenever a torque is applied to the wheel as it is essential for the friction generation at the tire-road interface in order to move forward. The steady-state correlation between slip ratio λ and friction coefficient μ is depicted in figure 2.1. The relationship is plotted for different road conditions. These curves are based on the *magic formula* (as called by many authors), which expresses the μ - λ relationship. Further details can be found in [12]. Slip above the optimum value μ_{max}, which strongly depends on the tire-road interface, will lead to reduced friction force and therefore reduced traction of the wheel.

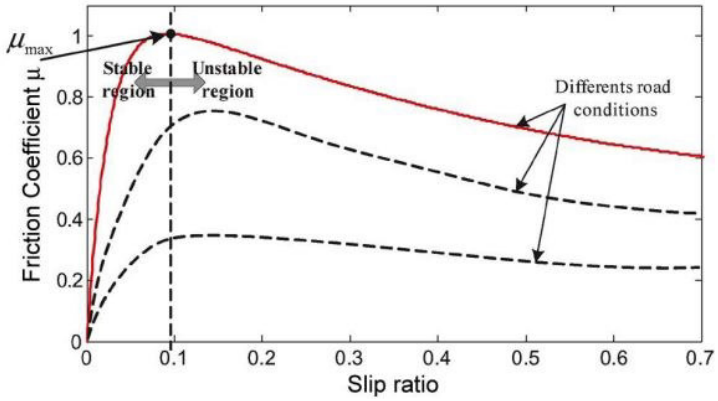

Figure 2.1: Magic formula $\mu - \lambda$ relationship; Source: [2]

Basic Requirements of a Slip Controller

The primary goal of slip control is therefore to modulate a control parameter (such as wheel torque or velocity) in a way that the friction force at the wheel maintains a maximum value according to the magic formula relationship. This will increase the controllability of the vehicle by avoiding slip. The control parameter has to be adjusted and updated while driving, e.g. online, as the road conditions - and with it the optimal slip ratio - can change very quickly. It is important that in "normal" operating conditions, where a torque is applied to the wheel which is less than the limit of the traction, the controller should not interfere in order not to limit the performance of the vehicle. Otherwise in critical situations, e.g. during sudden acceleration or deceleration or on slippery road conditions, the controller should limit wheel slip by adjusting the control parameter in the right way. Another requirement is that the controller should be robust to changes in external conditions because these conditions can change very quickly due to changes in velocity, soil and road conditions.

2.1.2 Longitudinal Motion Dynamics

As several in the following section described traction control strategies are based on the longitudinal motion of a vehicle, the equations of motion will quickly be presented. This is done according to [3] and with the help of figure 2.2. The description of the used symbols can be found in table 2.1.
In general, the longitudinal vehicle motion can be described with the following equations:

$$J_w\dot{\omega} = M - rF_d \tag{2.2}$$

$$m\dot{V} = F_d - F_{dr} \tag{2.3}$$

$$V_w = r\omega \tag{2.4}$$

$$F_d(\lambda) = \mu N \tag{2.5}$$

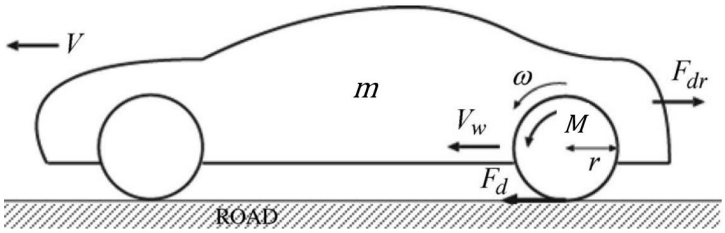

Figure 2.2: Longitudinal motion dynamics of a vehicle; Source: [3]

Table 2.1: Parameter list of the longitudinal motion equations; Source: [3]

Symbol	Definition
J_w	wheel inertia
V_w	wheel velocity
ω	wheel rotation
M	motor torque
r	wheel radius
F_d	driving / friction force
m	vehicle mass
N	normal force
V	chassis / vehicle velocity
F_{dr}	driving resistance
μ	friction coefficient

2.2 Different Traction Control Strategies

Within the scope of this thesis, different traction control concepts have been studied and compared. Figure 2.3 gives an overview of the in this section presented different control strategies. The classification of the strategies is inspired by [13] and has been extended and complemented by additional strategies, information and references.

2.2.1 Vehicle Speed Estimation

The designation *Vehicle Speed Estimation* names the "conventional" slip control strategy as it is often used for cars. It takes the approach of estimating the slip ratio (as introduced in equation 2.1) by measuring the wheel and vehicle speed and maintaining it at the optimal value by wheel speed control. This method has the advantage that it is quite easy to implement and to control compared to the other methods presented below, but it holds two basic problems. The first one is to obtain an accurate value for vehicle speed to calculate the slip ratio. According to [13], the simplest method to estimate the vehicle speed is to use position encoders on the non-driven wheels. This is not possible when the vehicle has an all-wheel drive or can brake with all wheels. Also, changes in tire rolling radius can cause additional errors ([14]).
Another method to measure the vehicle speed is the direct estimation from sensors mounted on the vehicle chassis. Different sensor types can be used in order to do that. Some examples are named in table 2.2.

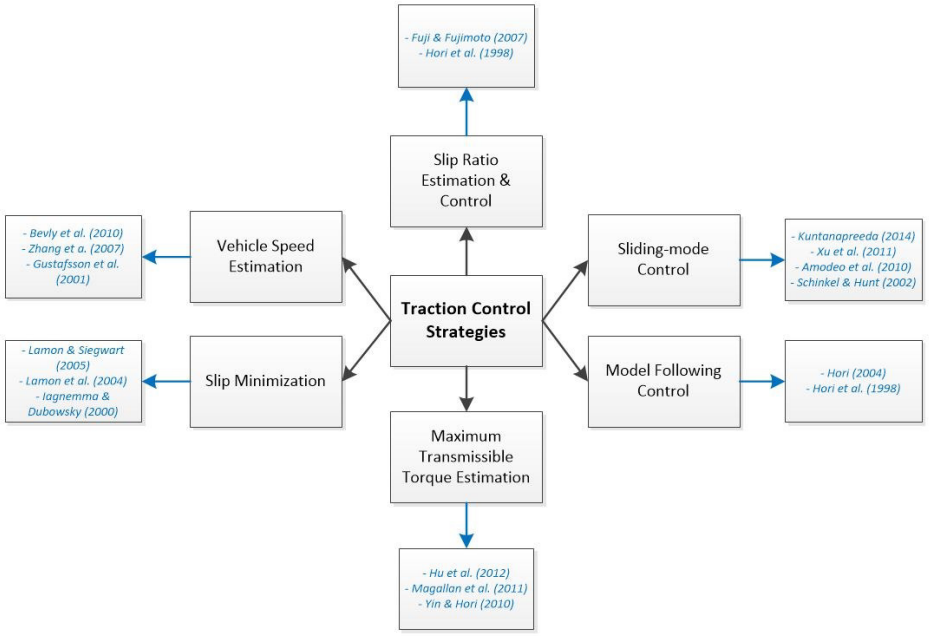

Figure 2.3: Overview different traction control strategies

Table 2.2: Different sensor types for vehicle speed estimation

Sensor Type	**Problems**	**Reference**
Accelerometer	accuracy is affected by speed offset due to long-time integral calculation	[4]
Optical sensors	robustness deteriorates over time due to dirt & soil ingress	[3]
Magnetic marker sensors	require a large change to road infrastructure	[3]
GPS	lost of signal in built up areas	[15]

As can be seen in table 2.2, using each sensor on its own comes with problems that prohibit receiving accurate results. That's why *sensor fusion* methods have been developed. They involve using signals from multiple sensors in combination with filters to compute the required parameters with higher accuracy. In order to estimate the vehicle speed, different strategies based on this method have been developed. For example, *Zhang et al.* [16] use a Recursive Least Squares (RLS) algorithm to estimate the vehicle speed from the wheel speed and an accelerometer signal. *Gustafsson et al.* [17] do almost the same but with a Kalman filter instead of RLS. By using a dynamic tire radius (radius changes during driving due to changing soil conditions), the results have shown that the vehicle speed estimation accuracy can be improved up to +/- 0.05 m/s.
Although an accurate vehicle speed value can be estimated by the help of sensor fusion, there is still a second problem: selecting a suitable slip ratio. As shown in section 2.1.1 the optimal slip ratio value is a function of the ground conditions. Estimating these conditions is one of the main problems that have to be solved to perform traction control. This deficit is attempted to be overcome by some of the following strategies.

2.2.2 Slip Ratio Estimation & Control

Slip Ratio Estimation

With the approach presented in this section, the slip ratio can be estimated without knowledge of the vehicle speed. This has the advantage that one does not have to worry about the accuracy of the vehicle speed and that less sensors have to be used in comparison to the Vehicle Speed Estimation method. The idea of this method will be explained based on the work of *Fujii & Fujimoto* [4]. It is based on the following differential equation of the slip ratio:

$$\dot{\lambda} = \frac{-\dot{\omega}}{\omega}\lambda + (1 + \frac{J_w}{r^2 m})\frac{\dot{\omega}}{\omega} - \frac{M}{r^2 m \omega} \tag{2.6}$$

This equation is derived from the vehicle's longitudinal motion equations presented in section 2.1.2 and describes the slip ratio changes of one wheel during driving.
With exception of λ, all parameters are assumed to be known or can be calculated from sensor signals, which means that the wheel speed ω and acceleration $\dot{\omega}$ have to be measured or estimated. According to [13], the advantage of this *Slip Ratio Estimation* (SRE) method is that these signals can be integrated from the wheel speed encoder to calculate the slip. By doing this, the signal noise can be reduced automatically.
The method has been tested experimentally with an electric vehicle during acceleration by *Fujii & Fujimoto* [4] and during urgent braking by *Suzuki & Fujimoto* [18]. The SRE has been developed into a non-linear slip controller based on feedback linearisation, which assumes a linearised relationship between slip and friction (will be discussed in the next section). The results show that although the slip ratio estimation is fast and accurate, the slip controller is only able to keep the slip ratio at +/- 0.3 of its reference value. This improves the slip behaviour, but the friction force will not be at its maximum value.
To conclude, one can say that this approach only improves the accuracy problem of vehicle speed estimation (since this value does not have to be measured) but still delivers no solution for the problem of varying road conditions. There is still no possibility of selecting the optimal reference slip ratio while driving.

Slip Ratio Control

As mentioned above, the SRE can be combined with a Slip Ratio *Control* method (SRC), which - as the name says - directly controls the slip ratio to achieve better traction results. Papers like [4], [19] and [5] have used this controller type. Here it will be presented according to the work of *Fujii & Fujimoto* [4], which uses a PI controller that considers small variations of the slip ratio around a chosen operation point. The structure of this controller can be found in figure 2.4.

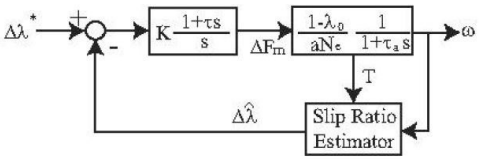

Figure 2.4: Block diagram of the SRC PI controller; Source: [4]

In order to design the slip ratio controller, the non-linearity in the μ - λ relationship should be linearised as follows:

$$\Delta\lambda = -\frac{1}{V_{w0}}\Delta V + \frac{V_0}{V_{w0}^2}\Delta V_w \tag{2.7}$$

where V_{w0} and V_0 are the wheel and vehicle speed at the chosen operation point, respectively. The gradient a_c of the μ - λ curve (which for example could be the magic formula presented in section 2.1.1) can be described by:

$$a_c = \frac{\Delta\mu}{\Delta\lambda} \tag{2.8}$$

Using the equations which describe the longitudinal motion of a vehicle (see section 2.1.2) in combination with equation 2.7, the transfer function of ΔF_m (describing the driver's acceleration command) to $\Delta\lambda$ can be obtained:

$$\frac{\Delta\lambda}{\Delta F_m} = \frac{1-\lambda_0}{a_c N_e}\frac{1}{1+\tau_a s} \tag{2.9}$$

with the time constant

$$\tau_a = \frac{J_n V_{w0}}{a_c N_e} \tag{2.10}$$

and the normal force N_e described by

$$\frac{1}{N_e} = \frac{1}{N}\frac{m}{J_n + m(1-\lambda_0)} \tag{2.11}$$

The vehicle can therefore be modelled as a first order system.

The PI controller can be unstable out of approximation errors. That is why *Fujii & Fujimoto* [4] also developed a non-linear controller based on feedback linearisation. Test results showed that this controller is more robust regarding modelling errors but the controller's reaction time is increased.

2.2.3 Sliding-mode Control

As the road conditions will always vary during driving and with it the tire-road interface, there will always be an uncertainty in the estimation of the optimal friction force in order to receive maximum traction in each driving situation. In order to account for this, an alternative to choosing a static reference slip ratio based on the peak friction coefficient predicted by the magic formula is the so-called *Sliding-mode Control* (SMC) method. With this control strategy, the desired slip ratio can be determined in real time and the received optimal value is taken directly as control target. Road estimation is included in this method in order to obtain different optimal slip ratios for different road conditions.
The method has been processed by authors like [2], [20], [21], [22], [23], [24], [25] and [26]. In this thesis, the idea of this method will be explained according to the information given by *Xu et al.* [26].
The SMC design can be derived by differentiating the wheel slip ratio in equation 2.1 with respect to the time. Considering the vehicle motion equations presented in section 2.1.2, the wheel slip dynamic equation during acceleration is obtained:

$$\begin{aligned}\dot{\lambda} = \frac{1}{\omega}\{\frac{F_{air}}{mr} - (1-\lambda)\frac{F_{res}r}{J} - [\frac{F_z}{mr} + (1-\lambda)\frac{F_z r}{J}]\mu + (1-\lambda)\frac{M}{J}\} \\ = f_1(\lambda) + f_2(\lambda)\mu + f_3(\lambda)M\end{aligned} \tag{2.12}$$

where

$$f_1(\lambda) = \frac{1}{\omega}[\frac{F_{air}}{mr} - (1-\lambda)\frac{F_{res}r}{J}] \tag{2.13}$$

$$f_2(\lambda) = -\frac{1}{\omega}[\frac{F_z}{mr} + (1-\lambda)\frac{F_z r}{J}] \tag{2.14}$$

$$f_3(\lambda) = \frac{1}{\omega}(1-\lambda)\frac{1}{J} \tag{2.15}$$

F_{air}, F_{res} and F_z are dynamic forces which act on the vehicle's wheels during driving. The non-linearities included in this system of equations are the slip ratio definition, the μ - λ relationship and the functions $f_1(\lambda)$ and $f_2(\lambda)$. In the corresponding paper [26], the authors focus on how to deal with the unknown friction coefficient μ. To do so, the so-called *sliding surface* is defined as:

$$s_{slide} = \lambda - \lambda_d \tag{2.16}$$

where λ_d denotes the desired wheel slip. Thus, the sliding surface s_{slide} can be defined as the "error" between the actual and the desired wheel slip, which we want to minimize. When differentiating s_{slide} and substituting it in the slip dynamic equation, the following equation is received:

$$\dot{s}_{slide} = \dot{\lambda} - \dot{\lambda}_d = f_1(\lambda) + f_2(\lambda)\mu + f_3(\lambda)M - \dot{\lambda}_d \tag{2.17}$$

With this information, the sliding condition can be found. *Xu et al.* [26] do this with the following inequalities:

$$\frac{1}{2}\frac{d}{dt}s_{slide}^2 \leq -\eta|s_{slide}| \quad or \quad \dot{s}_{slide} \leq -\eta \cdot sgn(s_{slide}) \tag{2.18}$$

where η is a strictly positive constant that depends on the vehicle's operating conditions and has to be figured out experimentally.
One problem of this approach is that chattering can occur during the driving operation. In order to avoid this, a continuous approximation of the sliding condition has to be used. This can be done by using a saturation function for the boundary layer instead of the sign function. By implementing this into equation 2.18 and solving it for the controller output torque M, the new equation looks as follows:

$$M = [-f_1(\lambda) - f_2(\lambda)\mu + \dot{\lambda}_d - \eta \cdot sat(\frac{s_{slide}}{\psi})]/f_3(\lambda) \tag{2.19}$$

where ψ is the boundary layer width which has to be chosen according to the frequency range for the corresponding dynamics. The received equation describes the motor torque that have to be applied to the wheel in order to avoid slip.
There are also alternatives how chattering can be avoided. For example, *Harifi et al.* [24] define *integral switching surfaces* which integrate λ instead of using a sign function.

Friction Coefficient Estimation

Since the friction coefficient $\mu(\lambda)$ is varying with the slip ratio, this coefficient has to be estimated. *Xu et al.* [26] do the estimator design with the help of the vehicle equations of motion (see section 2.1.2). According to [26], the friction coefficient can be obtained by dividing the driving force F_d by the normal force N. We get:

$$\hat{\mu} = \frac{\hat{F}_d}{N} = -\frac{J_w}{rN}\dot{\omega} + \frac{M}{rN} \tag{2.20}$$

As the estimator uses the first order derivative of the wheel rotation, a low pass filter should be added in order to avoid higher frequency noise.

Again, *Harifi et al.* [24] show an alternative to estimate this parameter. Their proposal is to use a tire-friction model based on parameters measured offline. The work provides the friction coefficient as a function of the wheel slip and the vehicle velocity:

$$\mu(\lambda, V) = (C_1(1 - e^{-C_2\lambda}) - C_3\lambda)e^{-C_4\lambda V} \tag{2.21}$$

where the constants C_i describe different properties of the μ-λ curve. *Harifi et al.* [24] have measured the values of these constants for a wide selection of road conditions.

The main advantage of this strategy is that it can keep the slip ratio at its desired value even when the friction coefficient between the tire and the road is altered as the vehicle moves over varying terrain. One drawback is that the measurement of the vehicle speed is required (see [20]).

2.2.4 Model Following Control

In [19] and [5], the idea of the *Model Following Control* method (MFC) can be found. The control strategy is developed and tested for the electric vehicle *UOT Electric March* and compared to the Slip Ratio Control strategy in [19].
The structure of the MFC feedback controller can be seen in the block diagram in figure 2.5.

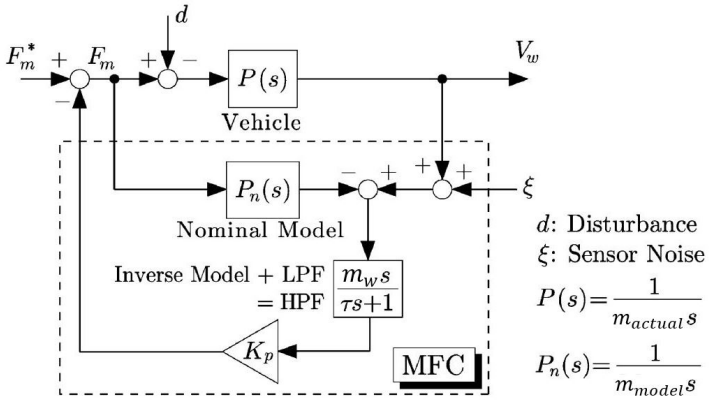

Figure 2.5: Block diagram of the MFC feedback controller; K_p: MFC gain, P & P_n: plants of vehicle and nominal model; Source: [5]

The parameter F_m^* denotes the acceleration command, controlled by the acceleration pedal of the vehicle driver.
The basic idea of this control strategy is that the complicated tire-road surface characteristics can be decoupled from the vehicle dynamics by modelling the multi-part vehicle as a single rigid body with equivalent inertia. This can be done by the help of the slip ratio λ, defined by equation 2.1. The relationship concerning this control idea is given by:

$$m_{actual} = m_w + m(1 - \lambda) \tag{2.22}$$

where m_{actual}, m_w and m are the total equivalent mass, the wheel mass and the equivalent vehicle mass (where "equivalent" means the equivalence of the mass to the inertia), respectively. This equation basically means that the vehicle seems to be lighter when λ (and so the wheel slip) increases. In other words, a rapid change

of the wheel velocity is observed as a sudden drop of the inertia.
Hori [5] use $m_{model} = m_w + m$ with $\lambda = 0$ as reference model (in figure 2.5 denoted as "nominal model"). When no slip occurs, m_{actual} is similar to m_{model}, which means that no control signal has to be generated by the MFC controller. Equation 2.3 is used to estimate the inertia of the nominal model.
In order to control wheel slip, the idea is that if the tire starts to slip, the actual wheel speed ω will increase quickly. However, the speed of the model will not increase. Thus, the difference between the actual wheel speed and the model speed can be fed back, and the controller can therefore react by reducing the motor torque, hence suppressing a sudden drop of inertia and reducing slip.
Hori [5] claims in his work that this control function is only needed for relatively high control frequencies. So they implemented a high-pass filter (HPF) into the feedback control path in order to handle just the needed frequencies.
The advantage of the MFC strategy is that it only considers the dynamics of the simplified system, avoiding the need to estimate slip or measure vehicle speed.

2.2.5 Maximum Transmissible Torque Estimation

The *Maximum Transmissible Torque Estimation* (MTTE) approach takes advantage of the features of electric driving motors to estimate the maximum transmissible output torque in order to avoid slip in real time, based on purely kinematic vehicle relationships. The proposed controller is able to follow this estimated value directly and constrains the torque reference in order to prevent slip. It uses the feedback computed from a simplified vehicle model to provide a saturation limit for the torque demand.
The only two parameters necessary to realize this prevention is the torque reference and the wheel speed in order to estimate the maximum transmissible torque to the specific road surface. This has the advantage that neither the chassis velocity nor information about complex tire-road conditions nor slip estimation are required.
Several papers like [27], [28], [29], [30], [2] and [31] address this control strategy. In this work, the strategy will be presented following *Yin et al.* [3]. For the description of the longitudinal motion of the vehicle, the differential equations derived in section 2.1.2 are used. For the interrelationships between slip ratio and friction coefficient, the magic formula presented in section 2.1.1 is used. The derived one-wheel vehicle model can be seen in the block diagram in figure 2.6.

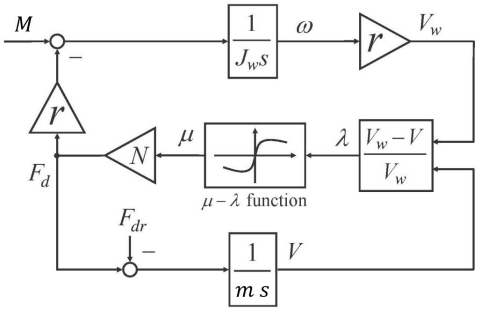

Figure 2.6: Block diagram of the one-wheel vehicle model with magic formula; Source: [3]

As we have learned in section 2.1.1, the difference between the velocities of the wheel and the chassis becomes larger as slip occurs. Together with the information of the magic formula, this leads to the conclusion that in this case the acceleration of the wheel becomes larger than that of the chassis as well. The basic idea of the

here presented strategy is that the condition for slip prevention is therefore that the acceleration of wheel and chassis have to be kept close together. Out of that, an appropriate relationship between these two accelerations have been developed in form of the following factor:

$$\alpha = \frac{\dot{V}^*}{\dot{V}_w^*} = \frac{(F_d - F_{dr})/m}{(M_{max} - rF_d)r/J_w} \tag{2.23}$$

This relaxation factor α is used to define the ratio of chassis and wheel acceleration $\dot{V}^*$ and $\dot{V}_w^*$, respectively. The values of this parameters do not have to be measured as they can be expressed by the vehicle's longitudinal motion equations (see equation 2.23). In order to satisfy the condition that slip does not occur, α should be close to one. Therefore, $\alpha = 1$ is the *no-slip condition* of this approach. We learn from this condition that for slip prevention, the maximum motor torque M_{max} must be reduced adaptively following the decrease of the friction force F_d as the road becomes more slippery.
By solving equation 2.23 for M_{max} and using the vehicle's longitudinal motion equations derived in section 2.1.2, the maximum transmissible torque can be estimated as:

$$M_{max} = (\frac{J_w}{\alpha m r^2} + 1) r F_d \tag{2.24}$$

where the friction force F_d acting on the wheel is

$$F_d = \frac{M}{r} - \frac{J_w \dot{V}_w}{r^2} \tag{2.25}$$

and can be concluded from the motion equations as well. These equations lead to the conclusion that a by the tire-road condition given F_d only allows a certain maximum wheel output torque as slip should not be increased.

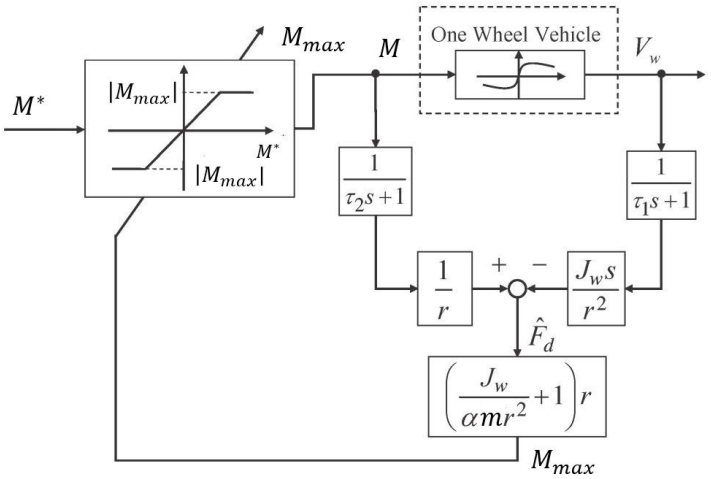

Figure 2.7: Control system based on MTTE; Source: [3]

The proposed design of the MTTE controller can be seen in figure 2.7. The estimator uses the measured values of the torque currently applied to the wheel as well as the current wheel speed to estimate the friction force as described in equation 2.25. In order to improve the wheel speed signal (e.g. generated by a shaft encoder) a low-pass filter (LPF) is implemented to smooth thE signal for the following differentiator. Another LPF is applied to the signal of M to keep the signals in phase.

The dashed block in figure 2.7 which describes the relationship between M and V_w is depicted in more details in figure 2.6. After a signal for F_d is derived, the maximum transmissible torque can be estimated using equation 2.24. Afterwards, a limiter realizes the torque control by limiting the torque output to the estimated value of M_{max}. The controller is therefore expected to just influence the system when necessary. Therefore, the whole system can basically be seen as a disturbance observer.

2.2.6 Slip Minimization Strategy

This strategy names a control concept presented by [32] and [33]. It is based on wheel-ground contact angle measurement and a numerical slip minimization algorithm. The greatest advantage is that it avoids relying on complex wheel-soil interaction models. It requires the formulation of a holistic model of the vehicle for optimized control of the wheel motor torques in order to minimize wheel slip. The idea of this strategy is based on the following derivation:

In general, a wheel is balanced – which means that no slip will occur – if the following inequality is fulfilled:

$$T \leq \mu_0 \cdot N \tag{2.26}$$

where T is the traction force (which is similar to the driving force F_d), μ_0 is the static friction coefficient and N is the normal force acting on the wheel. The traction force directly depends on the motor torque in the following way:

$$T = \frac{M}{r} \tag{2.27}$$

where M is the motor torque and r is the wheel radius.
In reality, it is very difficult to estimate μ_0 as it depends on the kind of wheel-ground interaction, which can change quickly while driving. Therefore, another way has to be found in order to avoid wheel slip. For that, it is first assumed that the wheel does not slip. It is then possible to calculate the forces T and N as a function of the motor torque. Afterwards, the results can be optimized by minimizing the ratio T/N. This ratio is similar to the friction coefficient as:

$$\frac{T}{N} = \frac{\mu_n \cdot N}{N} = \mu_n \tag{2.28}$$

By minimizing μ_n, the chances are optimized that this ratio is smaller than the real friction coefficient μ_0. If this is the case, no slip will occur.
As objective function of this optimization problem, the largest of all T/N ratios of all wheels have to be chosen because the probability that slip occurs at the corresponding wheel is the highest. The minimization is subject to constraints given by a vehicle model based on force balance equations. By solving this problem, the best possible torque distribution of all wheels in order to avoid slip is received. Additional information about this strategy can be found in chapter 3.
The main advantage of this strategy is that the probability that slip will occur can be minimized without knowing the real static friction coefficient.

2.3 Summary

As the conventional method to control wheel slip, a strategy based on vehicle speed estimation has been presented. As single sensors in order to estimate this value can not deliver enough accuracy, sensor fusion approaches have been developed which use a combination of several sensors and advanced filters to overcome this deficiency. As an alternative, approaches have been derived that directly estimate the slip ratio from its range of change and so avoid the measurement of the vehicle speed. This strategy can be combined with the SRC method which controls the slip ratio using a vehicle model based on longitudinal equations of motion. The disadvantage of both of these methods is that they can only rely on a static relationship between the slip ratio and the friction coefficient and so only one particular desired slip ratio can be chosen. Since this ratio varies while driving, it is not possible to achieve maximum traction forces all the time. That's why the sliding-mode control method has been developed. It can estimate the desired slip ratio in real time and takes it directly as control target on different surfaces. It has to be combined with a friction coefficient estimator. One has to be careful as chattering can occur with the use of this technique. The Model Following Control strategy only considers the dynamics of a system to make the slip ratio estimation redundant. It is based on the idea that the vehicle body can be simplified to a single inertia system which becomes "lighter" as the wheel slip increases. Another method based on a vehicle's model is the Maximum Transmissible Torque estimation strategy. The MTTE controller limits the torque the motor can apply to the wheel in order to limit wheel slip. As a last method, the idea of the Slip Minimization strategy has been presented. It is based on wheel-ground contact angle measurement and uses numerical algorithms in order to prevent slip before it occurs.

Chapter 3

Slip Minimization Strategy

As a result of the study and comparison of the different traction control concepts, the slip minimization strategy has been found to be the best suited of all possible solutions in order to control the traction behaviour of the walking excavator. In this chapter, the reasons why this strategy has been chosen will be explained in section 3.1. Afterwards, a quasi-static model of the excavator and a simulation in order to test this model will be presented in the sections 3.2 and 3.4. Section 3.3 describes the needed minimization algorithm of the strategy in more details.

3.1 Advantages

The slip minimization strategy has been chosen out of the following reasons:
First of all, the approach avoids relying on complex wheel-soil interaction models, whose parameters are generally unknown in challenging terrains. These parameters are on one hand very difficult to estimate and on the other hand only valid for a specific type of soil and vehicle conditions, which can change very quickly in reality. Furthermore, the conventional slip control methods account neither for a kinematic nor for a physical model. Out of that, the control parameters can just be updated when slip already occurred and thus the system can react only with a certain time delay. On the other hand, the slip minimization strategy targets to prevent slip before it occurs. That leads to more efficient motion and robustness.
Within the ongoing work of this project, force control tools have been developed that allow to actively adapt the excavator's chassis as a function of the terrain. The purpose of this is to optimize the ground reaction force distribution for better stability, less terrain damage and operation complexity reduction (further information in [9]). Out of that, it is possible to measure the forces acting on the excavator. This implementation gives great advantages regarding the estimation of the parameters that have to be measured in order to realize the slip minimization strategy on the walking excavator.
Another reason for this choice is that the chosen strategy uses torques as control parameters. In [33], torque control has been found to have a better performance compared to velocity control in our case, as the terrain becomes more challenging.

3.2 Excavator Model

As we have seen in chapter 2.2.6, the parameters T and N have to be determined in order to realize the slip minimization strategy. This determination requires a model of the vehicle. As a first approach how such a model of the walking excavator can look like, a planar, quasi-static model has been developed. This model is inspired

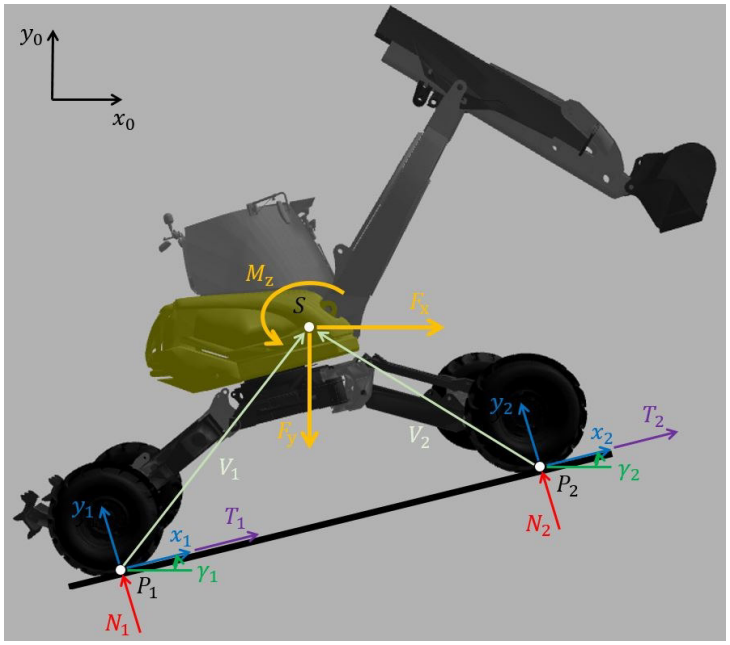

Figure 3.1: Model of the walking excavator

by *Iagnemma & Dubowsky* [34], who developed the same model for a wheeled rover. A planar system means that only forces in axial plane are considered. This is because of simplification and illustrative reasons. The system is assumed to be quasi-static, which means that all dynamic forces like forces due to acceleration, air and friction resistance are neglected. Additionally it is assumed that each wheel is in contact with the ground at one single point. This assumption is reasonable for vehicles with rigid wheels moving on firm terrain (according to [34]).
The parameters needed for the model are displayed in figure 3.1. These are the following ones:

- Vectors from the ground contact point to the excavator's center of mass are denoted by $\boldsymbol{V_i} = [V_i^x \quad V_i^y]^T$ where $i = 1, 2$ indicates the left or the right wheel, respectively. These vectors are expressed in the corresponding local coordinate system $\{x_i \quad y_i \quad z_i\}$ fixed at the ground-contact points P_i. x_i points tangential to the wheel-ground contact plane on which the corresponding wheel is driving, y_i stands perpendicular to x_i.

- The wheel-ground contact angles denoted by γ_i represent the angles between the horizontal and the wheel-ground contact plane.

- The vector $\boldsymbol{F} = [F_x \quad F_y \quad M_z]^T$ expresses the forces and the torque that are acting on the vehicle's center of mass. It represents the effects of gravitational and inertial forces and forces due to manipulation and interaction with the environment. This vector is expressed in the global coordinate system $\{x_0 \quad y_0 \quad z_0\}$.

- The wheel-ground contact forces which exist at each ground-contact point are denoted by the vector $\boldsymbol{f_i} = [T_i \quad N_i]^T$, expressed in the local coordinate system. It can be divided into the traction force T_i which points in the direction of x_i and the normal force N_i pointing in the y_i-direction. It is assumed that there are no torques acting at the wheel-ground interface.

With these definitions, the quasi-static force balance equations in x_0, y_0 and z_0 direction can be built:

$$cos(\gamma_1) \cdot T_1 - sin(\gamma_1) \cdot N_1 + cos(\gamma_2) \cdot T_2 - sin(\gamma_2) \cdot N_2 = F_x \tag{3.1}$$

$$sin(\gamma_1) \cdot T_1 + cos(\gamma_1) \cdot N_1 + sin(\gamma_2) \cdot T_2 + cos(\gamma_2) \cdot N_2 = F_y \tag{3.2}$$

$$V_1^y \cdot T_1 - V_1^x \cdot N_1 + V_2^y \cdot T_2 + V_2^x \cdot N_2 = M_z \tag{3.3}$$

This system of equations can be transformed into the following matrix form:

$$\begin{bmatrix} cos(\gamma_1) & -sin(\gamma_1) & cos(\gamma_2) & -sin(\gamma_2) \\ sin(\gamma_1) & cos(\gamma_1) & sin(\gamma_2) & cos(\gamma_2) \\ V_1^y & -V_1^x & V_2^y & V_2^x \end{bmatrix} \cdot \begin{bmatrix} T_1 \\ N_1 \\ T_2 \\ N_2 \end{bmatrix} = \begin{bmatrix} F_x \\ F_y \\ M_z \end{bmatrix} \tag{3.4}$$

One can see that the block matrices formed by the sine and cosine terms are simple rotational matrices in order to transform the ground-contact forces vector from local into global coordinates.
The equation system can be written in general matrix form:

$$G \cdot \boldsymbol{f} = \boldsymbol{F} \tag{3.5}$$

The matrix G is a function of the vehicle's center of mass, the wheel-ground contact locations P_i and the wheel-ground contact angles γ_i.

3.3 Minimization Algorithm

The information given in this section has been found in [32], [33] and [34], respectively.
The in equation 3.5 presented system of equations represents an under-constrained problem. This means that there are an infinite number of wheel-ground contact forces $\boldsymbol{f}$ that balance the vector $\boldsymbol{F}$. The purpose of the slip minimization strategy in order to control the traction behaviour of an vehicle is to choose a set of wheel-ground contact forces that satisfy the force distribution equations and some additional problem constraints while optimizing a specific criteria of system performance. As we have seen in chapter 2.2.6, this criteria is the minimization of wheel slip, which can be done by minimizing the ratio T/N. In order to do this minimization, the following optimization problem have to be solved:
We minimize the greatest of all T/N ratios of all wheels, because it has the highest risk that slip occurs at the corresponding wheel, subject to the previously established equation system 3.5. Additionally, two constraints have to be added. The first one is based on the goal of keeping all wheels in contact with the ground. Mathematically, this can be expressed by $N_i > 0$ for $i = 1, 2$.
The second constraint takes into account that the torque the wheel motors can provide is limited. Since the traction force directly depends on the motor torque in the way expressed by equation 2.27, the traction forces have to be constraint in the following way:

$$0 \leq T_i \leq T_{max} \tag{3.6}$$

T_{max} is the maximal output torque at the excavator's wheels divided by the wheel radius.

The complete mathematical notation of this minimization problem is therefore:

$$\begin{gathered} min\{max(\frac{T_i}{N_i})\}\ for\ i = 1,2 \\ s.t. \\ G \cdot \boldsymbol{f} = \boldsymbol{F} \\ N_1 > 0 \\ 0 \leq T_i \leq T_{max} \end{gathered} \tag{3.7}$$

As a solution of this problem, the ideal force distribution of the forces T_i and N_i in order to prevent slip is received.

3.4 Simulation

To check the functionality of the derived model, a simple MATLAB script was written. The script can be found in appendix A.
As a first step, the vectors pointing from the wheel-ground contact points to the vehicle's center of mass V_i and the wheel-ground contact angles γ_i have been assumed to be known. The algorithm was run for different configurations of these parameters. To solve the minimization problem, the MATLAB function *fmincon* was used. It is a non-linear programming solver based on the Interior Point Algorithm with the purpose to find the minimum of constraint non-linear multi-variable functions. Further information can be found in [35].
For the forces acting on the vehicle's center of mass $\boldsymbol{F}$, the following values were chosen:
F_x was set to zero as the system is assumed to be quasi-static, which means that all acceleration forces are neglected. F_y equals the vehicle's gravitational force, which is the total mass times the gravitational acceleration. M_z is zero since no torque occurs at the excavator's chassis.

Chapter 4

Results

In figure 4.1, the results of one MATLAB script run are plotted. The vehicle's center of mass was held constant in the middle of the two excavator wheels. The wheel-ground contact angles were varied from 0 to 45 degrees. This means that the inclination the excavator has to climb is continuously increased. The angles can be found on the axes of the single diagrams. Each diagram expresses the result of one wheel-ground contact force. The different colors describe the values of the forces at the corresponding angles, where blue denotes the minimum value (which is 0) and red the maximum value, which are T_{max} and N_{max}, respectively. For these values, reasonable numbers of the walking excavator have been chosen (exact values can be found in appendix A). In this example, the ratio T_1/N_1 was chosen as objective function of the minimization in order to test the model of the excavator (simulation results with ratio T_2/N_2 as objective function can be found in appendix B). In order to evaluate the results of this minimization problem, we will have a look at the special case where the ground-contact angles of both wheels are always equal. This case is denoted in the diagrams by the red lines. These values have been plotted with the angles in the x-direction and the absolute value of the wheel-ground contact forces in the y-direction. The result can be seen in figure 4.2.
One can see that this simple model works as the algorithm is able to keep the traction force T_1 close to zero as long as the ground-contact angles are not too high. As soon as the second traction force T_2 has reached its maximum value (denoted by the blue lines), T_1 starts to increase as well. This makes sense as T_2 is not able to "hold" the excavator's weight alone for high inclinations.
By looking at the behaviour of the normal force N_1, one can see that it starts to decrease for high angles (denoted by the orange line). By the time N_1 starts to decrease the excavator would start skidding as its weight cannot fully be "hold" by the ground-reaction forces anymore.
N_2 stays more or less equal for all angles, which is the expected result because the vehicle's center of mass was kept in the middle between the two wheels and the objective function included just the normal force N_1. Plots with other parameter configurations can be found in appendix B.

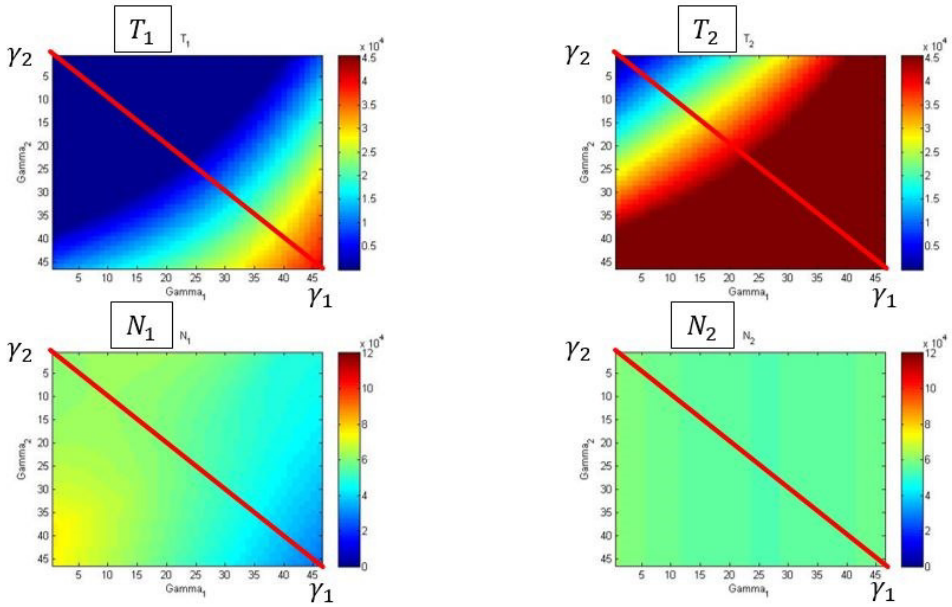

Figure 4.1: Simulation results for all ground-contact angles; Excavator's center of mass in the middle between the wheels; Objective function for minimization: T_1/N_1

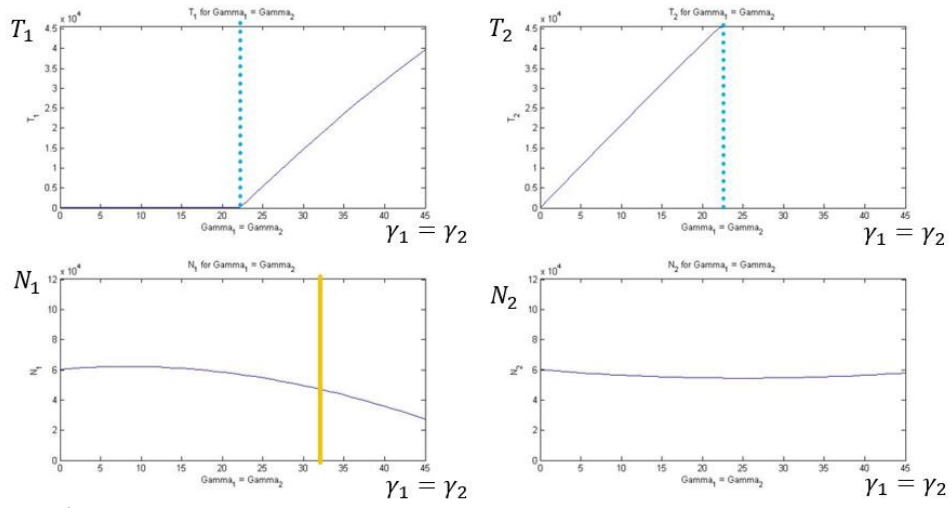

Figure 4.2: Simulation results for ground-contact angles $\gamma_1 = \gamma_2$; Excavator's center of mass in the middle between the two wheels; Objective function for minimization: T_1/N_1

Chapter 5

Conclusion and Future Work

In this thesis different traction control strategies have been studied and compared in order to increase the climbing abilities, control and performance of Muck Muck's walking excavator M545. As a result, the Slip Minimization strategy have been found to be the best suited one to optimize the excavator's traction behavior. As a first step to realize this concept, a planar quasi-static model of the excavator has been presented and tested with a simple MATLAB script.
The next steps of this project would be to extend this model in order to take dynamic effects into account. These effects come from acceleration, friction and air resistance and rolling resistance forces acting on the excavator while driving and become more important with higher velocities. Additional, the excavator's internal acting forces and torques (e.g. the torques at the different joints) could be included into the model to get a better description of the excavator's dynamic behaviour.
Another important point that the slip minimization strategy can work is the estimation of the wheel-ground contact angles, which have been assumed to be known in this thesis. The measurement or estimation of these angles is in general challenging because of the complex wheel-ground interactions and kinematic constraints. Real time estimation of these parameters is essential in order to achieve precise, robust autonomous guidance and control of the vehicle. There are several approaches how such an estimation can be done. For example, *Iagnemma & Dubowsky* [36] present a method using commonly available on-board sensors. The signals of these sensors are used with an algorithm based on rigid-body kinematic equations in combination with an extended Kalman filter to fuse noisy sensor signals.
The ground-contact angles can also be measured directly. *Lamon & Siegwart* [33] do this by direct measurement of the forces on the wheel periphery using flexible wheels equipped with deflection measuring sensors. The wheel-ground contact angle is then computed with a weighted mean of the sensor signals.
Another approach is to do the contact angle estimation visually. *Xu et al.* [37] presents an algorithm to do that. A monocular camera is required to be mounted on the front and the rear wheels. The field of view of these cameras have to contain the wheel-ground contact interface. Their locations relative to the wheels have to be known and fixed while the vehicle is driving. This configuration is used to measure the required angles with an edge detection strategy.
Furthermore, *Laohu et. al* [38] present a discrete Kalman filter based on wheel-ground contact angle and slip estimation scheme for their *lunar rover* by combining drive and guidance systems to form a closed loop system. In this system, the observer works out the slip values and wheel-ground contact angles by using the measured data of the passed route of the rover's center of mass.
In order to find the best possible strategy for the walking excavator, these strategies have to be evaluated and adapted to the excavator's problem.

Equally important is to find an optimization algorithm for the non-linear minimization problem that can solve it efficiently and online while driving. *Lamon & Siegwart* [33] and *Lamon et al.* [32] for example use a combination of different numerical optimization methods such as the Simplex, Fixed Point and Gradient method, which they apply in a specific sequence to achieve the best possible result. Furthermore, it would be interesting and necessary to compare the Slip Minimization strategy with another traction control concept (for example with the Vehicle Speed Estimation strategy). The strategies can be simulated and tested with the existing simulation framework for the walking excavator.

Bibliography

[1] Menzi Muck AG, "Homepage, Section *Schreitbagger*," http://www.menzimuck.com/produktgruppen/menzi-muck-schreitbagger/#fndtn-tab-1242, December 2015.

[2] G. Magallan, C. De Angelo, and G. Garcia, "Maximization of the Traction Forces in a 2wd Electric Vehicle," *IEEE Transactions on Vehicular Technology*, vol. 60, no. 2, pp. 369–380, Feb. 2011.

[3] D. Yin, S. Oh, and Y. Hori, "A Novel Traction Control for EV Based on Maximum Transmissible Troque Estimation," Jun. 2009.

[4] K. Fujii and H. Fujimoto, "Traction Control based on Slip Ratio Estimation Without Detecting Vehicle Speed for Electric Vehicle," in *Power Conversion Conference - Nagoya, 2007. PCC '07*, Apr. 2007, pp. 688–693.

[5] Y. Hori, "Future vehicle driven by electricity and Control-research on four-wheel-motored "UOT electric march II"," *IEEE Transactions on Industrial Electronics*, vol. 51, no. 5, pp. 954–962, 2004.

[6] Menzi Muck AG, "Homepage," http://www.menzimuck.com/home/, December 2015.

[7] S. Zimmermann, "Fast Driving Concepts for a Walking Excavator," December 2015, Studies on Mechatronics.

[8] ASL, "Robotic Systems Lab," http://www.rsl.ethz.ch/, ETH Zurich, December 2015.

[9] M. Hutter, P. Leemann, S. Stevsic, A. Michel, D. Jud, M. Hoepflinger, R. Siegwart, R. Figi, C. Caduff, M. Loher, and S. Tagmann, "Towards optimal force distribution for walking excavators," in *2015 International Conference on Advanced Robotics (ICAR)*, Jul. 2015, pp. 295–301.

[10] P. V. Osinenko, M. Geissler, and T. Herlitzius, "A method of optimal traction control for farm tractors with feedback of drive torque," *Biosystems Engineering*, vol. 129, pp. 20–33, Jan. 2015, 3.

[11] T. D. Gillespie, "Fundamentals of Vehicle Dynamics," SAE Technical Paper, Tech. Rep. R-114, Feb. 1992.

[12] H. B. Pacejka and R. S. Sharp, "Shear Force Development by Pneumatic Tyres in Steady State Conditions: A Review of Modelling Aspects," *Vehicle System Dynamics*, Jul. 2007.

[13] N. Ewin, "Traction Control for an Electric Vehicle," Tranfer Report, December 2011, Balliol College.

[14] A. Daiss and U. Kiencke, "Estimation of vehicle speed fuzzy-estimation in comparison with Kalman-filtering," in *, Proceedings of the 4th IEEE Conference on Control Applications, 1995*, Sep. 1995, pp. 281–284.

[15] D. M. Bevly, J. C. Gerdes, and C. Wilson, "The Use of GPS Based Velocity Measurements for Measurement of Sideslip and Wheel Slip," *Vehicle System Dynamics*, Aug. 2010.

[16] Q. Zhang, G. Liu, B. Liu, and X. Xie, "Sensor Fusion Based Estimation Technology of Vehicle Velocity in Anti-lock Braking System," 2007.

[17] F. Gustafsson, S. Ahlqvist, U. Forssell, and N. Persson, "Sensor Fusion for Accurate Computation of Yaw Rate and Absolute Velocity," SAE Technical Paper, Tech. Rep. 2001-01-1064, Mar. 2001.

[18] T. Suzuki and H. Fujimoto, "Slip ratio estimation and regenerative brake control without detection of vehicle velocity and acceleration for electric vehicle at urgent brake-turning." IEEE, Mar. 2010, pp. 273–278.

[19] Y. Hori, Y. Toyoda, and Y. Tsuruoka, "Traction control of electric vehicle: basic experimental results using the test EV "UOT electric march"," *IEEE Transactions on Industry Applications*, vol. 34, no. 5, pp. 1131–1138, Sep. 1998.

[20] M. Amodeo, A. Ferrara, R. Terzaghi, and C. Vecchio, "Wheel Slip Control via Second-Order Sliding-Mode Generation," *Intelligent Transportation Systems, IEEE Transactions on*, vol. 11, no. 1, pp. 122–131, Mar. 2010.

[21] A. Šabanovic, "Variable Structure Systems With Sliding Modes in Motion Control - A Survey," *IEEE Transactions on Industrial Informatics*, vol. 2, no. 7, pp. 212–223, 2011.

[22] V. Utkin, "Variable structure systems with sliding modes," *IEEE Transactions on Automatic Control*, vol. 22, no. 2, pp. 212–222, Apr. 1977.

[23] S. Kuntanapreeda, "Traction Control of Electric Vehicles Using Sliding-Mode Controller with Tractive Force Observer," 2014.

[24] A. Harifi, A. Aghagolzadeh, G. Alizadeh, and M. Sadeghi, "Designing a sliding mode controller for slip control of antilock brake systems," *Transportation Research Part C: Emerging Technologies*, vol. 16, no. 6, pp. 731–741, 2008.

[25] M. Schinkel and K. Hunt, "Anti-lock braking control using a sliding mode like approach," vol. 3. IEEE, 2002, pp. 2386–2391 vol.3.

[26] K. Xu, G. Xu, W. Li, L. Jian, and Z. Song, "Anti-skid for Electric Vehicles based on sliding mode control with novel structure." IEEE, Jun. 2011, pp. 650–655.

[27] J.-P. Yonnet, S. Hemmerlin, E. Rulliere, and G. Lemarquand, "Analytical calculation of permanent magnet couplings," *IEEE Transactions on Magnetics*, vol. 29, no. 6, pp. 2932–2934, Nov. 1993.

[28] J.-S. Hu, D. Yin, Y. Hori, and F.-R. Hu, "A new MTTE methodology for electric vehicle traction control," in *International Conference on Electrical Machines and Systems, 2009. ICEMS 2009*, Nov. 2009, pp. 1–6.

[29] Hu, Jia-Sheng and Yin, Dejun and Hori, Y. and Hu, Feng-Rung, "Electric Vehicle Traction Control: A New MTTE Methodology," *IEEE Industry Applications Magazine*, vol. 18, no. 2, pp. 23–31, Mar. 2012.

[30] J.-S. Hu, D. Yin, and Y. Hori, "Fault-tolerant traction control of electric vehicles," *Control Engineering Practice*, vol. 19, no. 2, pp. 204–213, Feb. 2011.

[31] D. Yin and Y. Hori, "Traction Control for EV Based on Maximum Transmissible Torque Estimation," *International Journal of Intelligent Transportation Systems Research*, vol. 8, no. 1, pp. 1–9, Jan. 2010.

[32] P. Lamon, A. Krebs, M. Lauria, R. Siegwart, and S. Shooter, "Wheel torque control for a rough terrain rover," in *2004 IEEE International Conference on Robotics and Automation, 2004. Proceedings. ICRA '04*, vol. 5, Apr. 2004, pp. 4682–4687 Vol.5.

[33] P. Lamon and R. Siegwart, "Wheel Torque Control in Rough Terrain - Modeling and Simulation," 2005.

[34] K. Iagnemma and S. Dubowsky, "Mobile Robot Rough-Terrain Control (RTC) For Planetary Exploration," 2000.

[35] MathWorks, "*fmincon*," http://ch.mathworks.com/help/optim/ug/fmincon.html?requestedDomain=ch.mathworks.com, December 2015.

[36] K. Iagnemma and S. Dubowsky, "Vehicle Wheel-Ground Contact Angle Estimation: With Application to Mobile Robot Traction Control." Springer Netherlands, 2000.

[37] H. Xu, X. Liu, H. Fu, B. B. Putra, and L. He, "Visual Contact Angle Estimation and Traction Control for Mobile Robot in Rough-Terrain," *Journal of Intelligent & Robotic Systems*, vol. 74, no. 3-4, pp. 985–997, Jul. 2013.

[38] Y. Laohu, L. Tun, Z. ZhiPing, and G. WeiPing, "Online estimation of wheel-ground contact angle and slip for a six-wheeled lunar rover," in *IEEE International Conference on Automation and Logistics, 2008. ICAL 2008*, Sep. 2008, pp. 2059–2063.

Appendix A

MATLAB Code

```
%%%%%% Simulation of Excavator M545 for Traction Control
%%%%% Bachelor Thesis - Simon Zimmermann - HS 15
%%%% Planar, quasi-static system - validity check - Final Version

%%% Tabula Rasa
clf
clc
close all

%%% Parameter definitions --> Indices 1->Wheel 1(left) / 2->Wheel 2(right -> front)
%% Vectors from ground-contact point to center of mass (Global Coo-Sys)
K = 1.650; % Adjustable range wheels [m]
L = 2.550; % Traveling height [m]
Q = 6.190; % Chassis length [m]
V_1_x_global = Q/3; % Absolute value from wheel 1 in x-direction [m]
V_1_y_global = K/5 + L/4; % Absolute value from wheel 1 in y-direction [m]
V_2_x_global = Q/3; % Absolute value from wheel 2 in x-direction [m]
V_2_y_global = K/5 + L/4; % Absolute value from wheel 2 in y-direction [m]

%% Constants
% Wheel radius
r_w = 1.14/2; % [m]

% Total vehicle mass
m_tot = 12300; % [kg] (without tools)

% Desired vehicle acceleration
a_des = 0; % [m/s^2] (quasi-static)

% Acceleration of gravity
g = 9.81; %[m/s^2]

% Maximum transmissible torque
M_max = 26000; % [Nm]

% Maximum transmissible traction force
T_max = M_max/r_w; % [N]

% Maximum normal force
N_max = m_tot*g; % [N]

%% Variables for opimization algorithm
% Force vector for forces on the vehicle's center of mass
F_x = m_tot*a_des; % Force in x-direction [N]
F_y = m_tot*g; % Force in y-direction [N]
M_z = 0; % Torque in z-direction [Nm]
```

```
F = [F_x; F_y; M_z];

% Lower bound
l_b = [0.1; 0.1; 0.1; 0.1];

% Upper bound
u_b = [T_max; N_max; T_max; N_max];

% Start values
x_0 = [0; 0; 0; 0];

%%% Solve System
% Start values
T_1 = T_max/2;
N_1 = m_tot*g/2;
T_2 = T_max/2;
N_2 = m_tot*g/2;

% Define Ratios:
Ratio_1 = T_1/N_1;
Ratio_2 = T_2/N_2;

% Check maximum ratio
if Ratio_1 > Ratio_2
    fun = @(x)x(1)/x(2);
elseif Ratio_2 > Ratio_1
    fun = @(x)x(3)/x(4);
else
    fun = @(x)x(1)/x(2);
end

% Check boundary conditions
if N_1 < 0 | N_2 < 0
    disp('ERROR: Normal forces are negative')
elseif T_1 < 0 | T_2 < 0
    disp('ERROR: Traction forces are negative')
elseif T_1 > T_max | T_2 > T_max
    disp('ERROR: Traction forces too high')
else
end

%% Solve non-linear optimization problem & track results
% Angle range (Gamma_1 & Gamma_2)
Angle_lim = 45;

% Tracking matrices (all values)
T_1 = zeros(Angle_lim+2,Angle_lim+2);
N_1 = zeros(Angle_lim+2,Angle_lim+2);
T_2 = zeros(Angle_lim+2,Angle_lim+2);
N_2 = zeros(Angle_lim+2,Angle_lim+2);

% Tracking vectors (values for Gamma_1 = Gamm_2)
T_1_v = zeros(1,Angle_lim+1);
N_1_v = zeros(1,Angle_lim+1);
T_2_v = zeros(1,Angle_lim+1);
N_2_v = zeros(1,Angle_lim+1);

for i = 0:Angle_lim

    % Update angle
    Gamma_1 = i;

    % Write angle into matrix
    T_1(i+2,1) = i;
    N_1(i+2,1) = i;
    T_2(i+2,1) = i;
    N_2(i+2,1) = i;
```

```
    for j = 0:Angle_lim

        % Update angle
        Gamma_2 = j;

        % Write angle into matrix
        T_1(1,j+2) = j;
        N_1(1,j+2) = j;
        T_2(1,j+2) = j;
        N_2(1,j+2) = j;

        %% Transformation of ground-contact vectors into local COO-SYS
        % Vector definition
        V_1_global = [V_1_x_global; V_1_y_global]; % vector from wheel 1
        V_2_global = [V_2_x_global; V_2_y_global]; % vector from wheel 2

        % Rotation matrices
        R_1 = [cosd(Gamma_1) sind(Gamma_1); -sind(Gamma_1) cosd(Gamma_1)];
        R_2 = [cosd(Gamma_2) sind(Gamma_2); -sind(Gamma_2) cosd(Gamma_2)];

        % Transformation
        V_1_local = R_1*V_1_global;
        V_2_local = R_2*V_2_global;

        % Components
        V_1_x_local = V_1_local(1);
        V_1_y_local = V_1_local(2);
        V_2_x_local = V_2_local(1);
        V_2_y_local = V_2_local(2);

        % Transformation matrix
        G = [cosd(Gamma_1) -sind(Gamma_1) cosd(Gamma_2) -sind(Gamma_2);...
        sind(Gamma_1) cosd(Gamma_1) sind(Gamma_2) cosd(Gamma_2);...
        V_1_y_local -V_1_x_local V_2_y_local V_2_x_local];

        % Solve non-linear omptimization problem
        options = optimoptions(@fmincon,'TolX', 10^-20);
        x = fmincon(fun, x_0, [], [], G, F, l_b, u_b, [], options);

        % Update of start value vector
        x_0 = [x(1); x(2); x(3); x(4)];

        % Track optimization results
        T_1(i+2,j+2) = x(1);
        N_1(i+2,j+2) = x(2);
        T_2(i+2,j+2) = x(3);
        N_2(i+2,j+2) = x(4);

        if Gamma_1 == Gamma_2
            T_1_v(1,i+1) = T_1(i+2,j+2);
            N_1_v(1,i+1) = N_1(i+2,j+2);
            T_2_v(1,i+1) = T_2(i+2,j+2);
            N_2_v(1,i+1) = N_2(i+2,j+2);
        end
    end
end

%%% Plot results
%% imagesc
figure(1)
subplot(2,2,1)
imagesc(T_1(2:Angle_lim+2,2:Angle_lim+2))
title('T_1')
xlabel('Gamma_1')
ylabel('Gamma_2')
colorbar
```

```
caxis([0 T_max])

subplot(2,2,2)
imagesc(T_2(2:Angle_lim+2,2:Angle_lim+2))
title('T_2')
xlabel('Gamma_1')
ylabel('Gamma_2')
colorbar
caxis([0 T_max])

subplot(2,2,3)
imagesc(N_1(2:Angle_lim+2,2:Angle_lim+2))
title('N_1')
xlabel('Gamma_1')
ylabel('Gamma_2')
colorbar
caxis([0 N_max])

subplot(2,2,4)
imagesc(N_2(2:Angle_lim+2,2:Angle_lim+2))
title('N_2')
xlabel('Gamma_1')
ylabel('Gamma_2')
colorbar
caxis([0 N_max])

%% Plots
x_axis = 0:1:45;

figure(2)
subplot(2,2,1)
plot(x_axis, T_1_v);
title('T_1 for Gamma_1 = Gamma_2')
xlabel('Gamma_1 = Gamma_2')
ylabel('T_1')
xlim([0 45])
ylim([0 T_max])

subplot(2,2,2)
plot(x_axis, T_2_v);
title('T_2 for Gamma_1 = Gamma_2')
xlabel('Gamma_1 = Gamma_2')
ylabel('T_2')
xlim([0 45])
ylim([0 T_max])

subplot(2,2,3)
plot(x_axis, N_1_v);
title('N_1 for Gamma_1 = Gamma_2')
xlabel('Gamma_1 = Gamma_2')
ylabel('N_1')
xlim([0 46])
ylim([0 N_max])

subplot(2,2,4)
plot(x_axis, N_2_v);
title('N_2 for Gamma_1 = Gamma_2')
xlabel('Gamma_1 = Gamma_2')
ylabel('N_2')
xlim([0 45])
ylim([0 N_max])
```

Appendix B

Additional Simulation Results

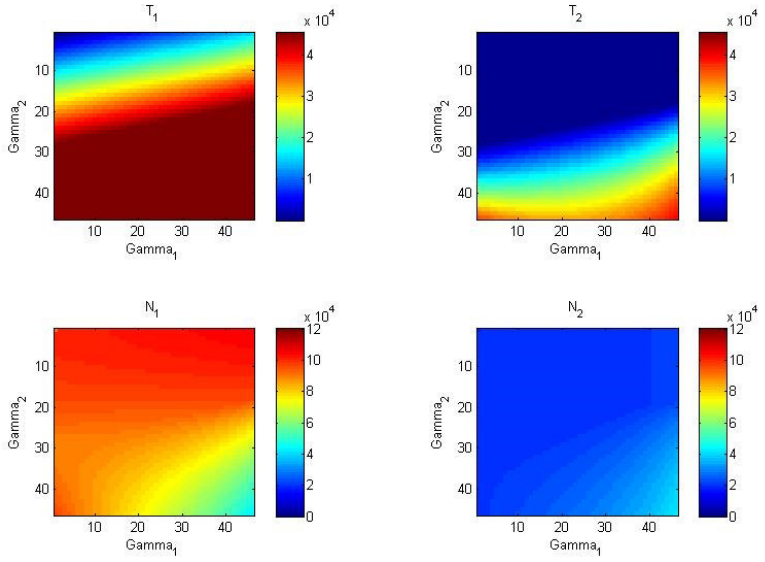

Figure B.1: Simulation results for all ground-contact angles; Excavator's center of mass close to rear wheel; Objective function for minimization: T_2/N_2

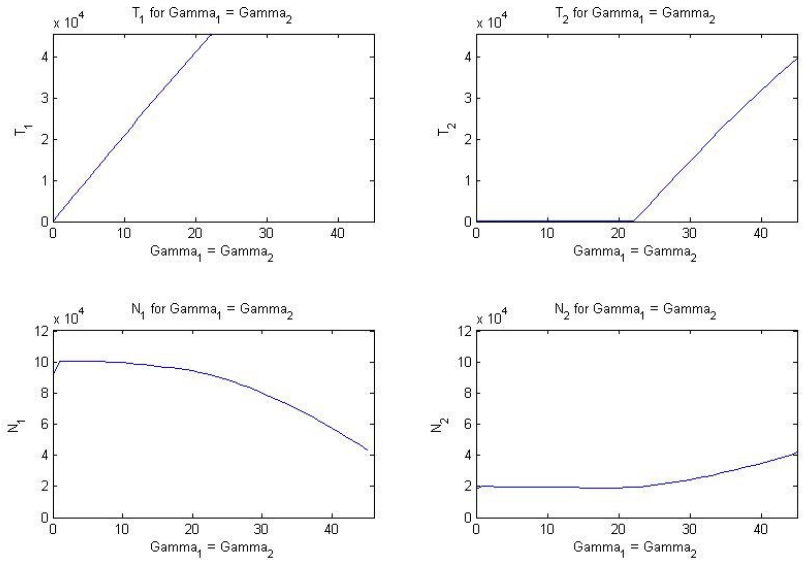

Figure B.2: Simulation results for ground-contact angles $\gamma_1 = \gamma_2$; Excavator's center of mass close to rear wheel; Objective function for minimization: T_2/N_2

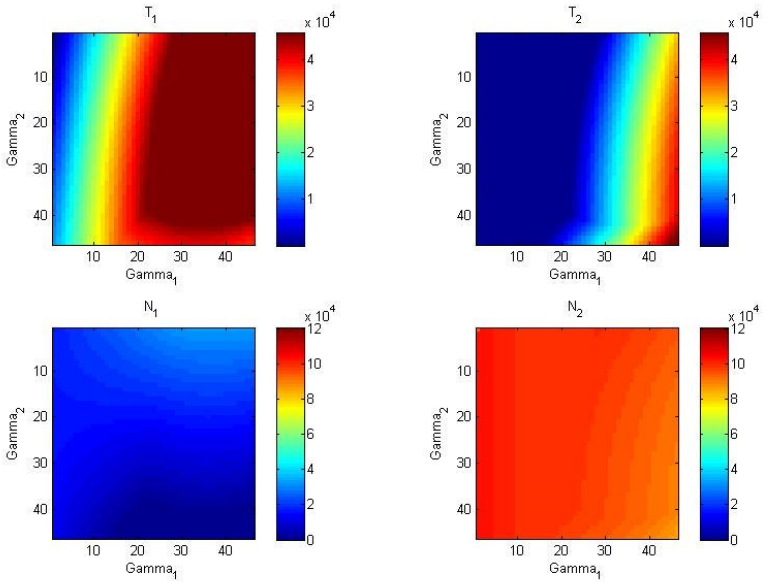

Figure B.3: Simulation results for all ground-contact angles; Excavator's center of mass close to front wheel; Objective function for minimization: T_2/N_2

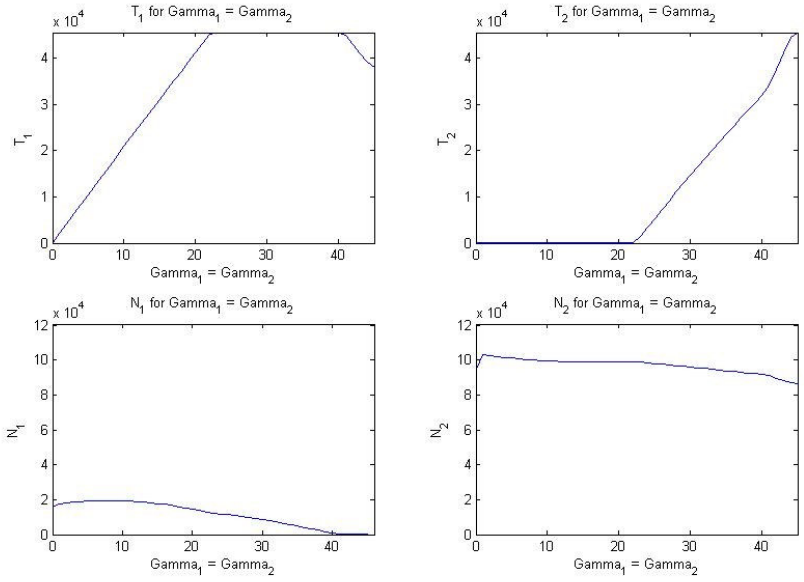

Figure B.4: Simulation results for ground-contact angles $\gamma_1 = \gamma_2$; Excavator's center of mass close to front wheel; Objective function for minimization: T_2/N_2